Polymer Vol. 38 No. 12, pp. 2867–2879, 1997

0032-3861/97/$17.00 + 0.00

PII: S0032-3861(96)00876-2

polymer papers

Crystal structural change in poly(3-alkyl thiophene)s induced by iodine doping as studied by an organized combination of X-ray diffraction, infrared/Raman spectroscopy and computer simulation techniques

Kohji Tashiro* and Masamichi Kobayashi
Department of Macromolecular Science, Faculty of Science, Osaka University, Toyonaka, Osaka 560, Japan

and Tsuyoshi Kawai and Katsumi Yoshino
Department of Electronic Engineering, Faculty of Engineering, Osaka University, Suita, Osaka 565, Japan
(Received 18 April 1996; revised 3 July 1996)

Preliminary results of the structural analysis of pristine and iodine-doped poly(3-alkylthiophene)s [poly(3-hexylthiophene) and poly(3-dodecylthiophene)] have been recorded by utilizing an organized combination of X-ray imaging plate and computer simulation techniques. The crystal structure of the pristine polymers was found to be composed of stacked layers constructed by a side-by-side arrangement of alkyl groups, where both the single and double layer structures were possible. The iodine-doped poly(3-alkylthiophene)s have been found to possess a tunnel structure produced by a cooperative translation of the polymer chains along the chain axis by half the repeating period, into which polyiodide ions such as I_3^- and I_5^- were trapped to form a charge-transfer complex with polythiophene skeletal chains. These structural changes were simulated by constructing energetically minimized crystal structural models, which gave X-ray fibre diagrams close to those of the observed ones. The infrared and Raman spectra were found to change in two stages during iodine doping, and the possibility of polaron and bipolaron species constructed by a combination of polythiophene and iodine ions was proposed. © 1997 Elsevier Science Ltd.

(Keywords: poly(3-alkylthiophene); crystal structure; iodine doping)

INTRODUCTION

Structural changes in the thermochromic phase transition of poly(3-alkylthiophene)s have been investigated extensively[1–6]. In a series of papers[2–4] we have studied the molecular and crystal structural changes in the thermochromic phase transition of poly(3-alkylthiophene)s of different alkyl side-chain lengths through X-ray diffraction, infrared spectra and visible–ultraviolet spectral measurements. In the temperature region of thermochromic phase transition, the alkyl side chains experience *trans–gauche* conformational disordering which induces twisting of the originally planar polythiophene skeletal chain, resulting in a change of electronic π–π conjugation length (*Scheme 1*). In this way the intercorrelation between the alkyl side chains and the thiophene skeletal chains is very strong.

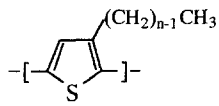

Scheme 1

In order to clarify this correlation more definitely, we have to obtain detailed information on the molecular and crystal structure. Many authors have proposed crystal structure models of poly(3-alkylthiophene) at room temperature[1,3,5–19]. For example, Winokur *et al.* utilized the Rietveld method and reproduced X-ray reflectional profiles[19]. But the structural variables used in their analysis were limited because the number of observed reflections was small. Therefore their proposed structure may not necessarily be reasonable from the energetic point of view. They also simulated the temperature dependence of the X-ray reflectional profiles by using rigid-rod models without taking into account any change of the alkyl side-chain conformation. Similarly, Luzny calculated the X-ray reflectional profile of poly(3-dodecylthiophene) under the assumption that the perfectly flat monomers of alkylthiophene are linked to form a polymer chain with the intermonomer deflection angle θ, and estimated the value of θ by fitting the

* To whom correspondence should be addressed

calculated pattern to the observed one[20]. This treatment is unreasonable, judging from the spectroscopic data which showed clearly the *trans*-to-*gauche* conformational change in the alkyl side chains. Besides, the models constructed by these two groups are quite different from each other. In spite of these significant problems, however, their simulated X-ray patterns are almost perfectly coincident with the observed data. This might originate from a situation such that the number of observed X-ray reflections is too small to determine the structural parameters uniquely. In this sense, therefore, the crystal structure of poly(3-alkylthiophene) has not yet been definitely established.

The crystal structure of poly(3-alkylthiophene) changes not only in the thermochromic phase transition but also in the process of doping ionic species into polymer samples. When iodine, for example, is doped into poly(3-alkylthiophene)s, the electric conductivity is enhanced remarkably[21]. In order to clarify the correlation between polythiophene, alkyl side groups and dopant molecules in the realization of high electric conductivity, information on the structural change before and after doping is very important. Winokur *et al.* proposed to elucidate the structural change induced by iodine doping by fitting X-ray equatorial reflectional profiles[7]. But the iodine ions cannot be located in this early-proposed structure because no vacant space is allowed, as is discussed in the present paper. In a recent paper[22], Tashiro *et al.* proposed a large structural change before and after iodine doping into the pristine (i.e., undoped) poly(3-alkylthiophene)s: the molecular chains shift along the chain axis and large tunnels are generated between the polymer skeletons and the layers of alkyl side chains, in which the long iodine ions such as I_3^- and I_5^- can be located well enough. This idea of structural change was supported by a large change in the X-ray fibre diagram and the infrared and Raman spectra. Winokur *et al.* revised their initial structural model of doped poly(3-alkylthiophene)s[23], which is essentially the same idea as that proposed by Tashiro *et al.*[22], and fitted the observed X-ray data relatively well. But in this case, also, they employed molecular chain models with limited structural variables, and so the proposed models might not be energetically stable.

In a series of papers[24–26] we developed a new system of structural analysis of polymer crystals, in which the X-ray imaging plate is used for taking the fibre photographs and the initial structure necessary for structural refinement is generated by a direct method used in the automatic structural analysis of low-molecular-weight single crystals or by a computer-aided molecular design technique. This technique is considered to be useful also for the structural investigation of the present polymers.

As already reported briefly, we constructed energetically optimized crystal structural models and compared the observed X-ray diffraction patterns with those simulated by these models[27,28]. In this paper we report preliminary results of the structural analysis of poly(3-alkylthiophene) crystals before and after iodine doping by combining the X-ray diffraction and infrared/Raman data with the computer simulation technique in an organized manner. The samples used were mainly poly(3-hexylthiophene) (P3HT, $n = 6$) and poly(3-dodecylthiophene) (P3DT, $n = 12$). Other members of the poly(3-alkylthiophene)s were also used to check the reasonableness of the structural models obtained.

EXPERIMENTAL

Poly(3-alkylthiophene)s were cast from chloroform solution at room temperature and stretched on a hot stage to about 4–5 times their original length. Iodine doping was performed by immersing the films into $KI–I_2$ aqueous solution for a predetermined period of time. Then the samples were taken out of the solution and the surfaces were rinsed lightly with methanol and wiped clean with filter paper.

The doped samples were sealed into glass capillaries in order to avoid sublimation of iodine molecules from the samples and taken for X-ray diffraction measurement.

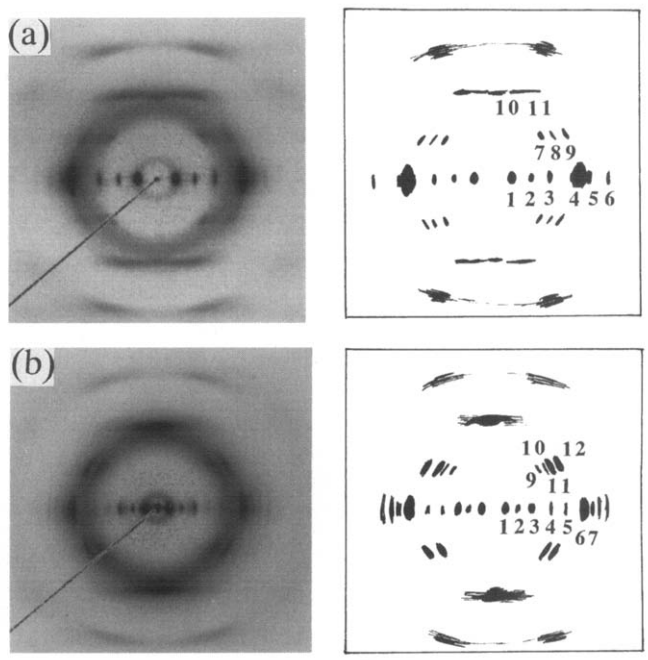

Figure 1 X-ray fibre diagrams of (a) P3HT and (b) P3DT. In order to clarify the reflectional positions, the illustrations are shown on the right side of these diagrams. The number of reflections is referred to in *Tables 1* and *2*

Table 1 Lattice spacing and relative intensity of the observed and calculated[a] reflections of P3HT

No.[b]	Indices	d_{obs} (Å)	d_{calc} (Å)	I_{obs}[c]	I_{calc}	
1	1 0 0	16.63	17.46	vs	100%	
2	2 0 0	8.32	8.73	s	7	
3	3 0 0	5.54	5.82	s	21	
4	0 2 0	3.88	4.27	vs	5	(23)[d]
	1 −2 0		4.21		18	
5	1 2 0	3.65	4.09	m	3	(22)
	2 −2 0		3.93		19	
6	3 −2 0	3.38	3.54	w	43	(44)
	5 0 0		3.49		1	
7	1 −1 −1	5.23	5.56	m	14	(28)
	1 −1 1		5.51		14	
8	2 −1 −1	4.63	4.91	m	7	(14)
	2 −1 1		4.88		7	
9	3 −1 −1	3.89	4.18	m	4	(8)
	3 −1 1		4.17		4	
10	1 0 −2	3.77	3.80	w	5	
11	2 0 −2	3.52	3.56	w	3	

[a] The calculated values are for model 3, shown in *Figure 5*
[b] Numbering of the reflections is indicated in *Figures 1, 8* and *17*
[c] Relative intensity: vvs, very very strong; vs, very strong; s, strong; m, medium; w, weak
[d] The values shown in parentheses are the total intensities summed up for the possible (or overlapped) reflections

Table 2 Lattice spacing and relative intensity of the observed and calculated[a] reflections of P3DT

No.[b]	Indices	d_{obs} (Å)	d_{calc} (Å)	I_{obs}[c]	I_{calc}	
1	1 0 0	25.70	25.65	vvs	100%	
2	2 0 0	13.05	12.82	s	44	
3	3 0 0	8.63	8.55	vs	71	
4	4 0 0	6.39	6.41	w	15	
5	5 0 0	5.16	5.13	w	17	
6	0 2 0	3.90	4.12	vs	18	(82)[d]
	1 −2 0		4.11		16	
	1 2 0		4.02		4	
	2 −2 0		4.01		44	
7	7 0 0	3.70	3.66	w	1	
8	4 −2 0	3.24	3.59	w	78	(125)
	6 −2 0	3.00	3.08	w	47	
9	0 1 1	5.47	5.68	w	8	(21)
	0 1 −1		5.63		5	
	1 −1 −1		5.60		4	
	1 −1 1		5.57		4	
10	2 −1 −1	4.97	5.28	w	27	(43)
	2 −1 1		5.27		16	
11	3 1 1	4.57	4.65	m	3	(5)
	3 1 −1		4.58		2	
12	4 −1 1	4.07	4.36	vs	98	(160)
	4 −1 −1		4.35		62	

[a] The calculated values are for model 3, shown in *Figure 6*
[b] Numbering of the reflections is indicated in *Figures 1* and *9*
[c] Relative intensity: vvs, very very strong; vs, very strong; s, strong; m, medium; w, weak
[d] The values shown in parentheses are the total intensities summed up for the possible (or overlapped) reflections

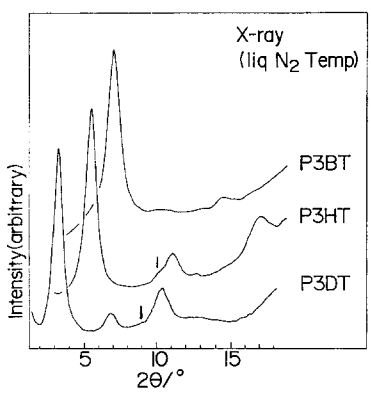

Figure 2 X-ray reflectional profiles measured at low temperature for a series of P3AT samples [P3BT: poly(3-butyl thiophene)]

Measurements of X-ray fibre diagrams were carried out using an MAC Science imaging plate system (DIP 1000). Fourier-transform infrared spectra of the pristine and doped films were measured with a Japan Spectroscopic Company *FT*i.r. 8300 spectrophotometer and also a Bio Rad FTS -60A/896 *FT*i.r. spectrometer. The resonance Raman spectra of the pristine and doped films were measured with a Japan Spectroscopic Company R1000 Raman spectrophotometer with an excitation beam from an argon-ion laser of wavelength 514.5 nm.

RESULTS AND DISCUSSION

Structure analysis of pristine poly(3-alkyl thiophene)s

X-ray fibre diagrams. *Figure 1* shows the X-ray fibre diagrams taken by DIP 1000 at room temperature for the uniaxially oriented P3HT and P3DT samples. In *Tables 1* and *2* are listed the observed lattice spacings and the relative intensities of the observed reflections of these two samples. In our previous paper[3], we indexed the

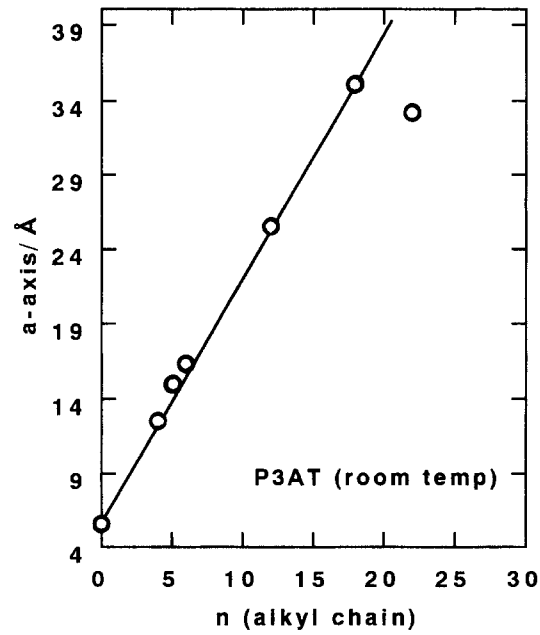

Figure 3 Relationship between *a*-axial length and carbon number of the alkyl side chains of a series of P3AT

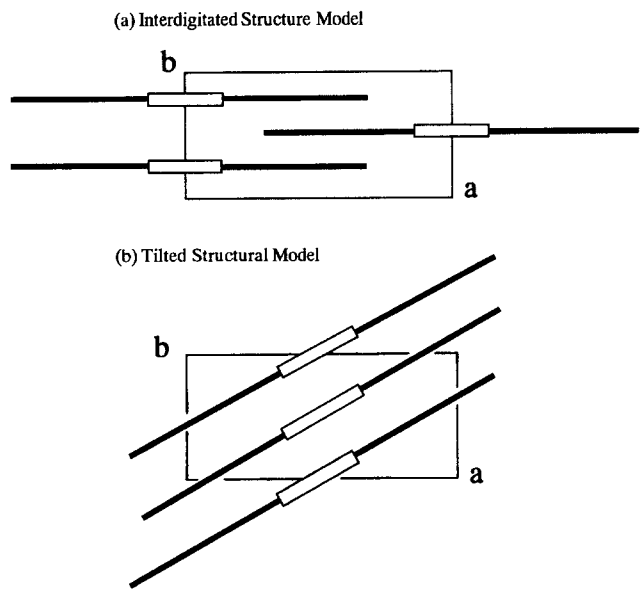

Figure 4 Two possible packing modes of P3AT

observed reflections of these two samples on the basis of the following orthogonal unit cells:

$$\left.\begin{array}{l}\text{P3HT } (n=6)\\ \quad a=16.63\,\text{Å},\ b=7.75\,\text{Å},\ c\text{ (fibre axis)}=7.77\,\text{Å}\\ \text{P3DT } (n=12)\\ \quad a=25.83\,\text{Å},\ b=7.75\,\text{Å},\ c\text{ (fibre axis)}=7.77\,\text{Å}\end{array}\right\} \quad (1)$$

But, as seen in *Figure 2*, where the equatorial reflectional profiles are shown, the weak reflections can be detected clearly in the low scattering angle region, but their intensities are too low to observe in the normal photograph as reported in the previous paper[3]. The fibre photographs shown in *Figure 1* were obtained by subtracting the background coming from air scattering and so have higher clarity than the photographs reported in the previous paper[3], making it possible to find the very

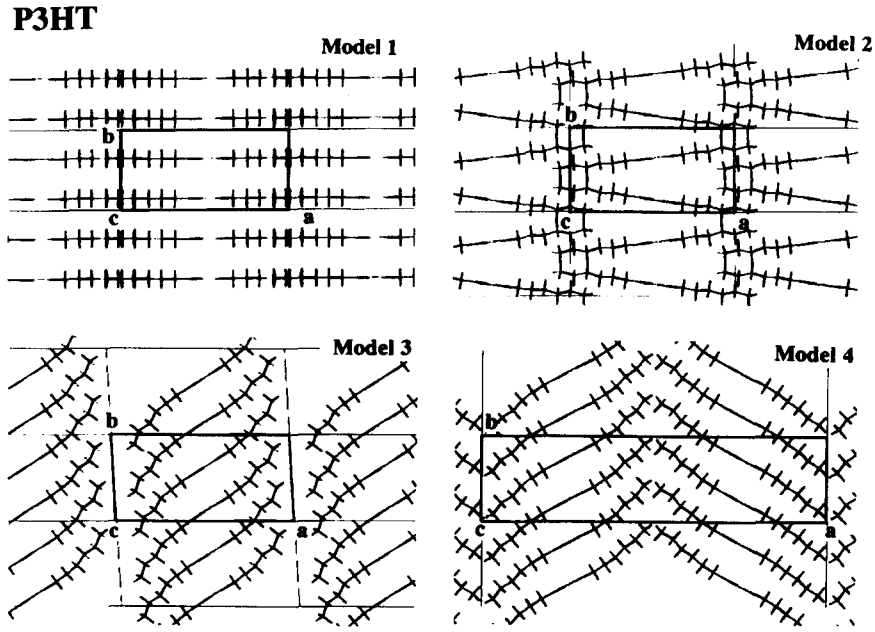

Figure 5 Energetically minimized packing models of P3HT

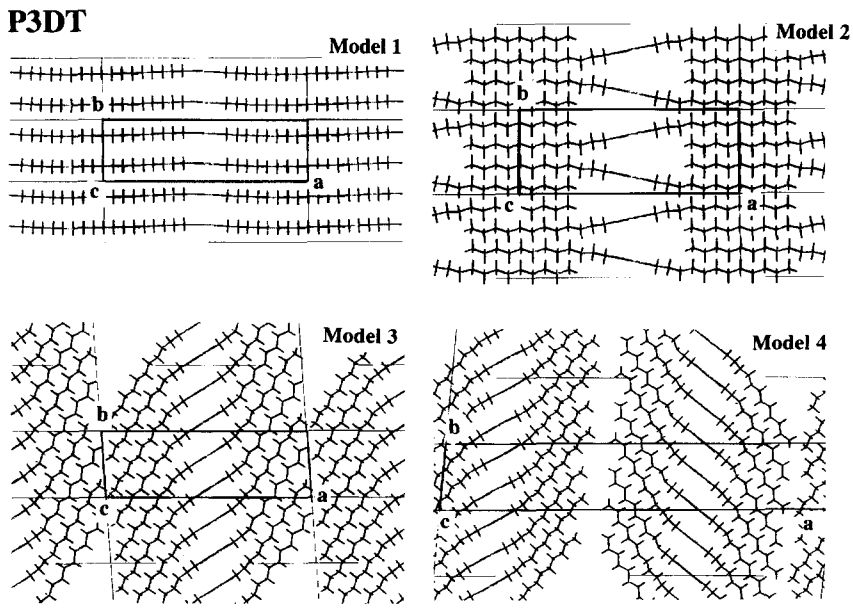

Figure 6 Energetically minimized packing models of P3DT

weak reflections shown in *Figure 2*. By taking into account these weak reflections, we have to enlarge the *a* axial length to twice the value indicated in equation (1):

$$\left.\begin{array}{l}\text{P3HT } (n=6)\\ \quad a=33.26\,\text{Å},\ b=7.75\,\text{Å},\ c\text{ (fibre axis)}=7.77\,\text{Å}\\ \text{P3DT } (n=12)\\ \quad a=51.66\,\text{Å},\ b=7.75\,\text{Å},\ c\text{ (fibre axis)}=7.77\,\text{Å}\end{array}\right\} \quad (2)$$

These unit cell parameters are in agreement with those reported by Winokur *et al.*, although they doubled the *a* axial length without any experimental evidence. Of course we have another possibility, that the basic unit cell is that shown in equation (1) and the doubled cell structure of equation (2) is generated as a result of, for example, a stacking disorder of layers or disorder within the layers themselves. Detailed discussion will be given in a later section.

Modelling of structure. As indicated in the previous paper[3], the alkyl side groups take essentially the *trans*-zigzag conformation, although some *gauche* bonds are included as a disordered part at room temperature. At low temperatures such as liquid nitrogen temperature, the conformation becomes almost perfectly of the all-*trans* type. The repeating period along the chain direction, 7.77 Å, suggests a fully extended planar conformation of the polythiophene skeletal chain. By taking into account these basic structures of the constituent parts of the chain, i.e. the conjugated structure of the skeletal chain combined with the all-*trans* conformation of the side chains, the span from one end of the alkyl side chain to the other end via the polythiophene skeletal chain is estimated to be ca. 22 Å for P3HT and ca. 36 Å for P3DT. In *Figure 3* is plotted the *a* axial length (of the basic unit cell, equation (1)) against the number of alkyl carbon atoms *n*. The increasing rate of the *a* axis

per two methylene atoms, i.e. the pitch of a pair of CH_2 groups, is ca. 1.62 Å/(2CH_2). Because the CH_2 group of the planar-zigzag conformation has an effective length of ca. 1.27 Å along the chain axis, the pitch should be 2.54 Å/(2CH_2) if the alkyl side chains are oriented along the *a* axis. The observed pitch of 1.62 Å/(2CH_2) is too short compared with the calculated value. Taking this situation into account, the following two packing modes of the side chains may be possible as the basic structure:

(1) The neighbouring two chains are arranged in parallel along the *a* axis and the side chains are interdigitated to each other, as shown in *Figure 4a*.
(2) The chains are gathered together to form a layer structure with the plane of the chain tilted from the *a* axis by an angle of $\cos^{-1}(1.62/2.54) = 50°$, as shown in *Figure 4b*.

Starting from the structural idea illustrated in *Figure 4*, energetically stable packing structures were constructed. For example, *Figures 5* and *6* illustrate the energetically minimized packing structures of P3HT and P3DT, respectively. All these models were obtained by using the commercially available program 'Polygraf' (version 3.22, Molecular Simulations Inc., USA). The potential functions used were of the Dreiding II type[29]. The atomic charges were calculated on the basis of the Q-equilibrate method[30]. The electrostatic interaction energy was calculated on the basis of the Ewald method. Minimization was performed by the conjugate gradient algorithm under the condition of convergence criterion of both the root-mean-squared total force and the unit cell stress lower than 0.001 kcal mol^{-1} Å^{-1}. The cell parameters obtained are as shown in *Table 3* (in model 4, the *a* axial length is twice the value of the other models).

Table 3 Cell parameters of energetically stable models and actual observations

		a (Å)	*b* (Å)	*c* (Å)	α (°)	β (°)	γ (°)	Total energy (kcal mol^{-1})
P3HT	model 1	16.12	7.77	7.92	90.3	89.7	89.8	151.18
	model 2	16.09	8.28	7.87	89.7	89.7	90.5	165.51
	model 3	17.49	8.56	7.80	89.4	90.0	93.3	162.98
	model 4	33.37	8.31	7.80	89.7	89.8	90.0	306.83 (153.42 × 2)
	observed	16.63 (33.26)	7.75	7.77	90.0	90.0	90.0	
P3DT	model 1	26.18	7.91	8.10	90.9	89.8	90.8	195.83
	model 2	23.42	9.98	7.85	88.2	90.0	90.0	157.16
	model 3	25.71	8.26	7.78	89.5	89.4	94.1	151.54
	model 4	52.08	8.74	7.78	89.1	88.9	84.6	322.77 (161.39 × 2)
	observed	25.83 (51.66)	7.75	7.77	90.0	90.0	90.0	

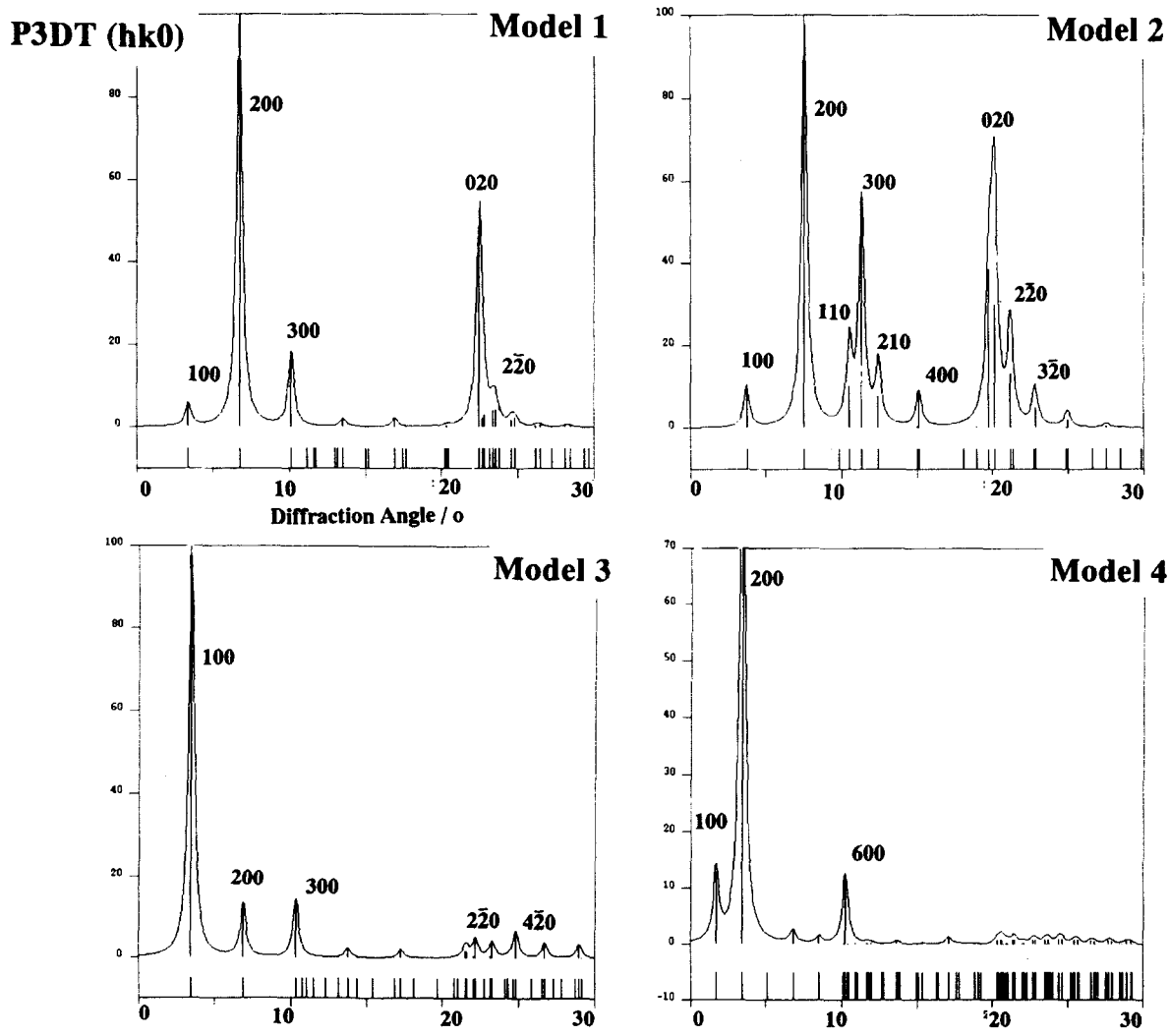

Figure 7 X-ray reflectional profiles simulated for the various packing models of P3DT

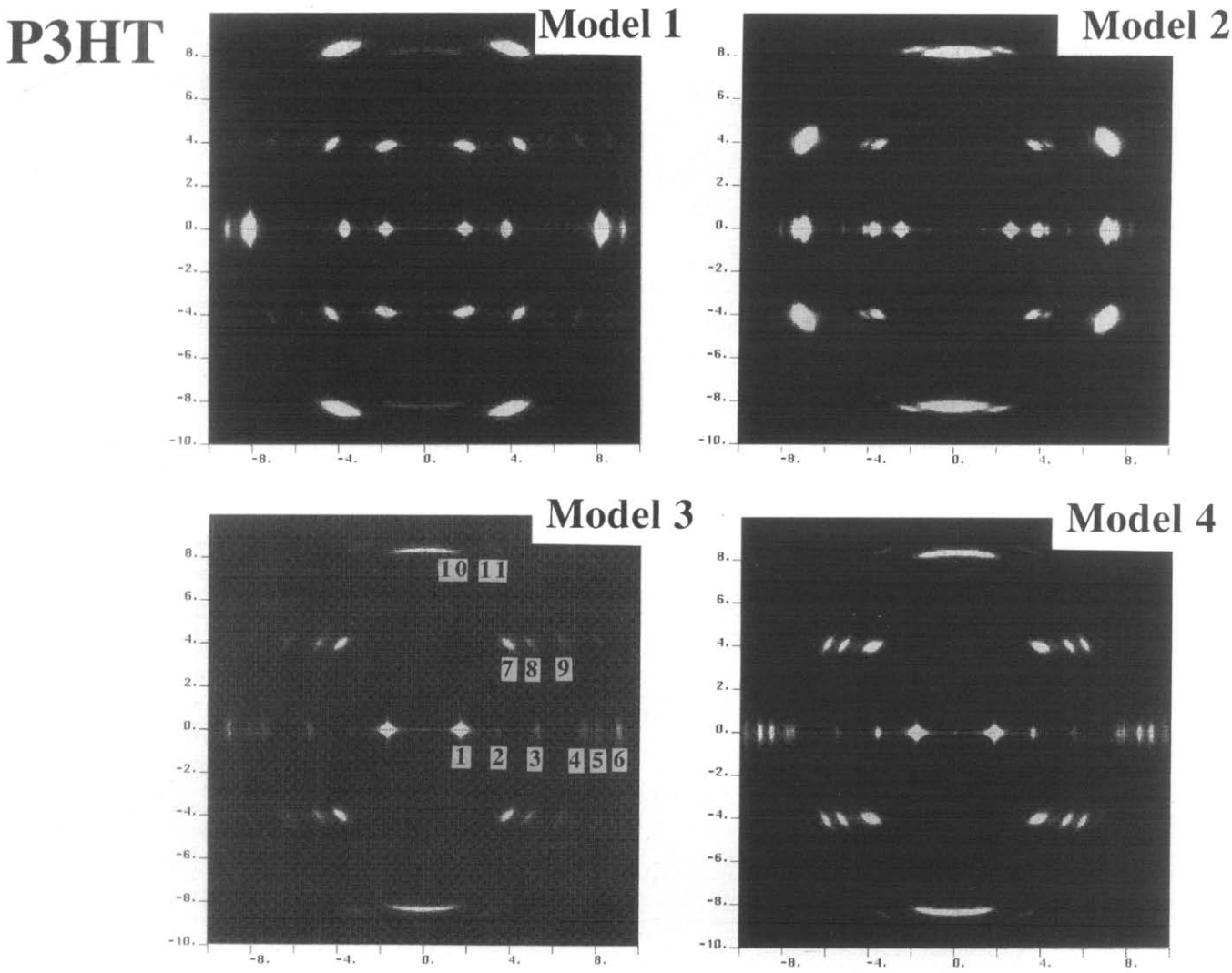

Figure 8 X-ray fibre diagrams simulated for the various packing models of P3HT. The numbering of the reflections is referred to in *Figure 1* and in *Table 1*

In models 1 and 2, the thiophene rings of the neighbouring chains are packed closely along the *b* axis and the *trans*-zigzag alkyl side chains are interdigitated partly along the *a* axis and form the well-packed subcell structure. The relative height of the neighbouring chains is different by one-quarter of the *c* axis length in model 1. In model 2 the thiophene rings are arranged side-by-side with a relative height difference of one-half the *c* axis, and the thiophene planes deflect as a whole slightly from the *a* axis direction, although the alkyl side chains are packed in parallel along the *a* axis. Models 3 and 4 consist of stacked layers, each of which is constructed by a parallel array of adjacent chains along the *b* axis with a tilt angle from the *a* axis of ca. 50°. This tilt angle is very close to that evaluated from *Figure* 3. Model 3 is of the one-layer type and model 4 is of the double-layer type, corresponding to that proposed by Winokur *et al.*[7,19].

X-ray fibre diagrams and equatorial profiles were calculated for these structural models by using the program 'Cerius^2' (version 2.0; Molecular Simulation Inc.), in which the size of the crystallites was assumed to be 200 Å in the *a*, *b* and *c* directions. The degree of orientation of the crystallites was assumed to be 4°. Temperature factors of 5 Å^2 were assumed for all the carbon and sulfur atoms. In *Figure 7* are shown the calculated X-ray reflectional profiles of the equatorial line of these four models of P3DT. Through comparison with the data actually observed, models 3 and 4 were extracted as the most plausible candidates for the structure. As indicated above, these two models are energetically stable. The reflectional positions are not perfectly in coincidence with the observed peaks, because the cell parameters optimized are at 0 K but the observed data were obtained at room temperature. In the present study we tried to obtain structural models which gave X-ray profiles as similar as possible to the observed patterns in a qualitative or semi-quantitative manner. As a problem to be solved in the near future, however, we have to modify the potential functions used in the calculation of the structural models so as to reproduce quantitatively the experimental data such as the one-dimensional and two-dimensional X-ray diffraction patterns and the infrared and Raman spectral data.

Figures 8 and *9* show the calculated X-ray fibre diagrams for models 1–4 of P3HT and P3DT, respectively. In model 1 the relative intensity of the innermost reflection of the first layer line is too high compared with the observed one, and in model 2 the outermost reflection of the first layer line is too strong and cannot reproduce well the observed intensity. Models 3 and 4 give simulated fibre diagrams relatively closer to those of

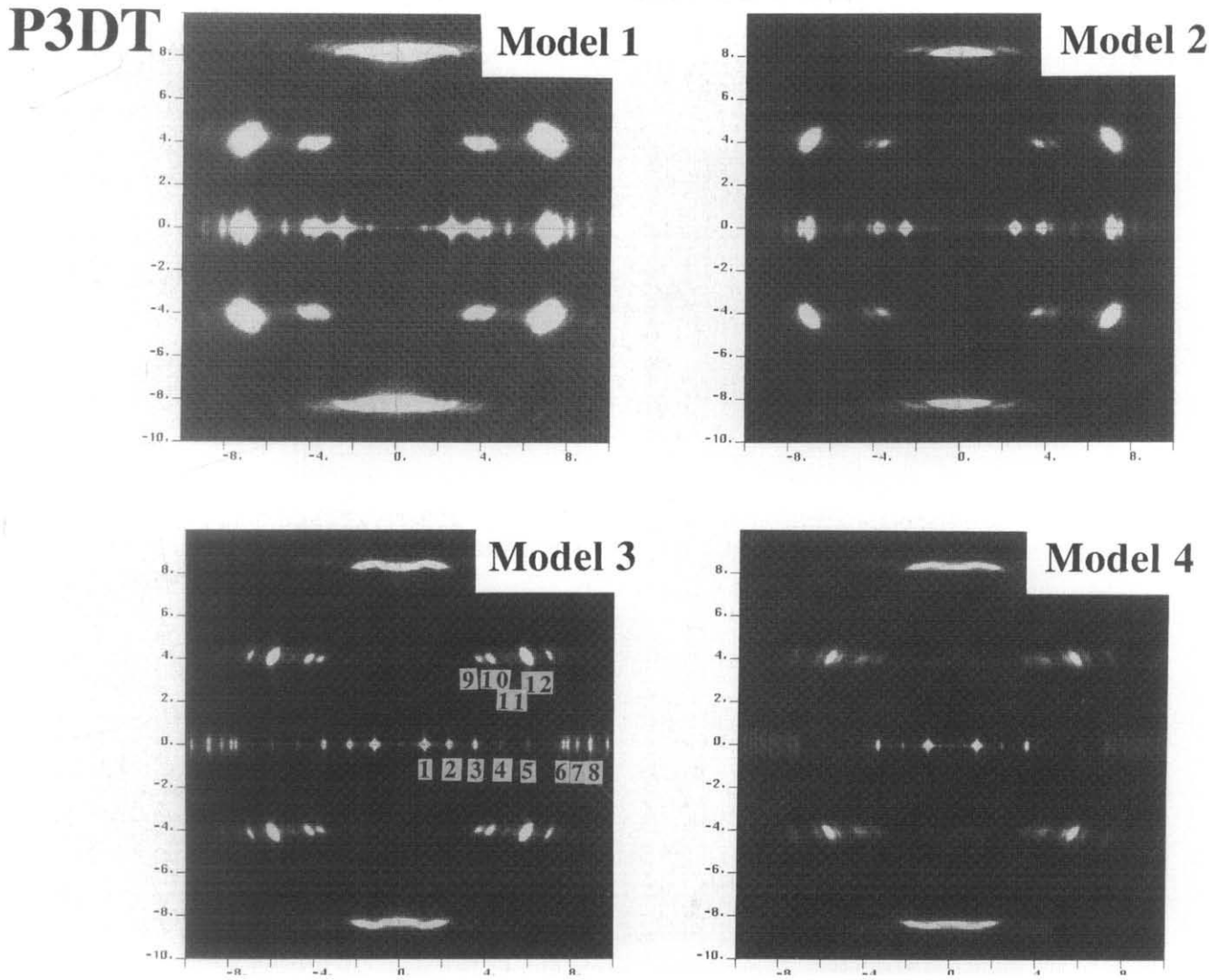

Figure 9 X-ray fibre diagrams simulated for the various packing models of P3DT. The numbering of the reflections is referred to in *Figure 1* and in *Table 2*

the observed ones, not only for the equatorial reflections but also for the layer lines, although a large discrepancy, can still be seen for some reflections (for example, Nos. 4 and 6 in Table 1 and Nos. 7, 8 and 11 in Table 2 where the numbering is referred to in *Figure 1*).

In this way, models 3 and 4 seem plausible from the viewpoint of X-ray diffraction and energy calculation. It should be noted here that, as suggested already, the regularly stacked layer structure of models 3 and 4 does not, in principle, give the odd-numbered $h00$ reflections due to the systematic extinction rule. Therefore we cannot distinguish only on the basis of the X-ray diffraction data which is the best one between models 3 and 4. If some stacking disordering occurs in the crystal (for example, .../\/\/////////\/\/\/\ ..., where / and \ represent layers of the same internal structure stacked in the opposite way), or if the two adjacent layers are slightly different in the internal structure, then the $h00$ reflections of h = odd can appear with relatively weak intensities. In model 4 of P3DT, for example, the minimized structure has some difference in the adjacent layers, resulting in the observation of additional reflections of h = odd with weak intensities. Such a difference was not seen for the model 4 P3HT crystal. From these discussions, we may speculate that P3DT, with longer alkyl side chains, might cause some disordering in the internal structure of layers more easily than in the case of P3HT with its relatively short side chains.

Structural change induced by iodine doping

X-ray fibre diagrams. *Figure 10* shows the X-ray fibre diagrams of the uniaxially oriented P3HT samples taken before and after doping of iodine[23]. The pattern of the doped samples is quite different from that of the original one. From these diagrams some characteristic features may be picked out. (1) The orientation of the polythiophene chain is preserved even after doping. (2) Position and relative intensity of the equatorial reflections are remarkably different from those of the pristine samples, indicating that the lattice structure projected along the chain axis changes drastically with doping. (3) Intense new reflections can be seen on the first layer line. They are indexed as *101* and *011* reflections, as indicated in *Table 4*, where the reflectional indices are on the basis of the unit cell parameters of the one-layer structure as shown in equation (1). Additionally, some diffuse scatterings are observed on the equatorial line and also at the positions between the first and second layer reflections, suggesting the appearance of a superlattice

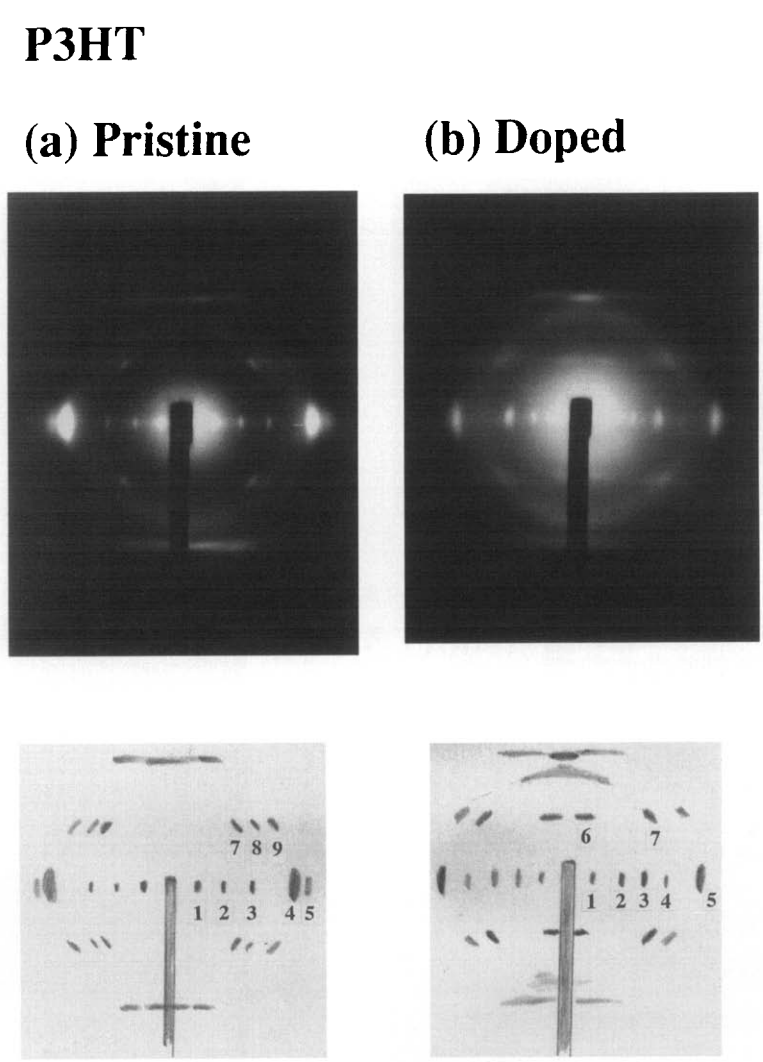

Figure 10 X-ray fibre diagrams of (a) pristine and (b) iodine-doped P3HT samples. The numbering of the reflections is referred to in *Table 4*

structure as a result of iodine invasion into the original crystal structure. (4) The spacings between the layer lines are almost the same as those of the original one, indicating that the fibre repeating period is essentially the same before and after doping.

All the reflections in *Figure 10* can be assigned on the basis of the following unit cell parameters:

Undoped
$a = 16.63$ Å, $b = 7.75$ Å, c (fibre axis) $= 7.77$ Å (33.26 Å)
Doped
$a = 37.25$ Å, $b = 23.15$ Å, c (fibre axis) $= 7.77$ Å

The unit cell of the doped sample corresponds in size to six basic cells, where model 3 is taken for the basic unit cell, i.e. two cells in the a direction and three cells in the b direction (if the unit cell of model 4 is taken as the basic cell, the lattice is three times larger than the original cell but only in the b direction). In *Table 4* are listed the indices and lattice spacings observed for the doped sample. The size of the basic cell itself is also modified to some extent after doping: the a axis $= 37.25/2 = 18.63$ Å, which is approximately 2 Å longer than the original value, and the b axis $= 23.15/3 = 7.72$ Å, slightly shorter than the original b axis. But it should be noted that the a axial length changes apparently continuously, depending on the doped ion concentration, as pointed out by Winokur *et al.*[7].

Infrared and Raman spectral changes induced by iodine doping. *Figure 11* shows the time dependence of the Fourier-transform infrared spectra taken for the unoriented P3HT films during the iodine doping treatment. The spectra change in two stages. At the first stage broad bands (asterisks in *Figure 11*) begin to appear and increase in intensity. As the doping proceeds further, the intensity of these broad bands continues to increase and at the same time new intense bands begin to appear at different wavenumber positions (double asterisks). Corresponding to these changes, the bands of the original polythiophene skeletal chain change drastically: for example, the band of 1510 cm^{-1}, characteristic of the thiophene ring mode, decreases in intensity and becomes broader. In contrast, the infrared bands, characteristic of the side-chain alkyl groups, do not change. We should note here that the infrared spectra are almost the same between the samples doped by immersing into the KI–I_2 solution and by exposing into the I_2 gas atmosphere. Polarized infrared spectral measurements revealed that most of the new bands show clear parallel dichroism along the chain axis, as shown in *Figure 12*. This clear polarization character, in addition to the well-oriented X-ray fibre pattern, is evidence for the formation of a crystalline complex while the chain orientation stays unchanged. As shown in *Figure 13*, the wavenumbers of these infrared bands are different from each other between the doped PT and P3HT but are close between

Table 4 Comparison of lattice spacing and relative intensity between the observed data and those calculated[a] for the energetically minimized model of iodine-doped P3HT

No.[b]	Indices	d_{obs} (Å)	d_{calc} (Å)	I_{obs}[c]	I_{calc}	
1	200	18.55	17.52	vs	100	
	300	12.46	11.68	w	0	
2	400	9.35	8.76	m	50	
	500	7.59	7.01	w	0	
3	600	6.29	5.84	s	91	
4	630	4.73	4.67	m	2	
5	930	3.59	3.46	s	1	(82)[d]
	1000		3.50		33	
	6 −60		3.49		48	
6	101	7.51	7.61	s	0	(39)
	011		7.49		3	
	01 −1		7.46		36	
7	621	4.36	4.33	m	0	(4)
	531		4.36		0	
	611		4.65		4	
	241		4.47		0	
8	202	3.85	3.82	w	13	(14)
	112		3.85		1	
9	312	3.67	3.67	w	1	(1)
	122		3.72		0	
10	703	2.33	2.31	w	0	(0)
	623		2.33		0	
	533		2.33		0	

[a] The calculated values are for model shown in *Figure 16b*
[b] Numbering of the reflections is indicated in *Figures 10* and *17*
[c] Relative intensity: vvs, very very strong; vs, very strong; s, strong; m, medium; w, weak
[d] The values shown in parentheses are the total intensities summed up for the possible (or overlapped) reflections

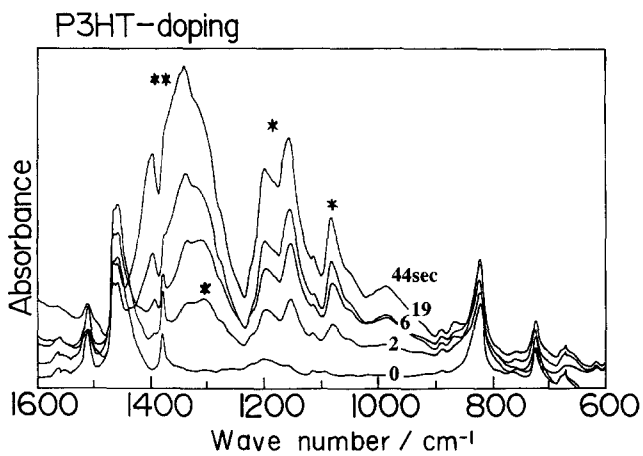

Figure 11 Time dependence of infrared spectra of iodine-doped P3HT sample

P3HT and P3DT, suggesting that the structural change caused by iodine doping may differ in the mode between PT and P3HT (and P3DT). In other words, the alkyl side groups seem to play some important role in the formation of the iodine complex of P3HT and P3DT.

Figure 14 shows the Raman spectra of the P3HT sample measured before and after doping, where the wavelength of the excitation laser beam is 514.5 nm, almost coincident with the absorption peak for the doped sample; thus the bands associated with the electronically conjugated skeletal chain and the iodine groups are enhanced remarkably due to the resonance effect. As the doping proceeds, the thiophene-ring mode at about 1450 cm^{-1} shifts by approximately 10 cm^{-1} toward the higher frequency side, consistent with the change in the conjugated structure of the

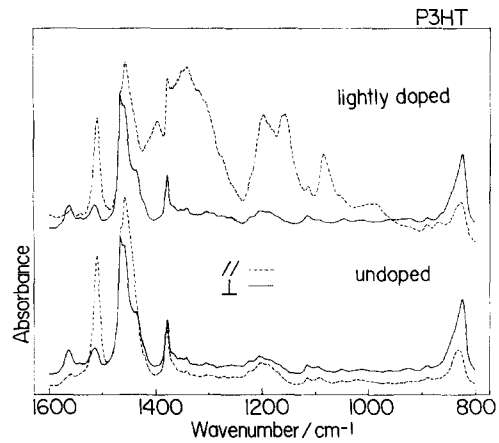

Figure 12 Polarized infrared spectral change before and after iodine doping in P3HT. The electric vector of the incident infrared beam is perpendicular (—) or parallel (- - -) to the chain axis

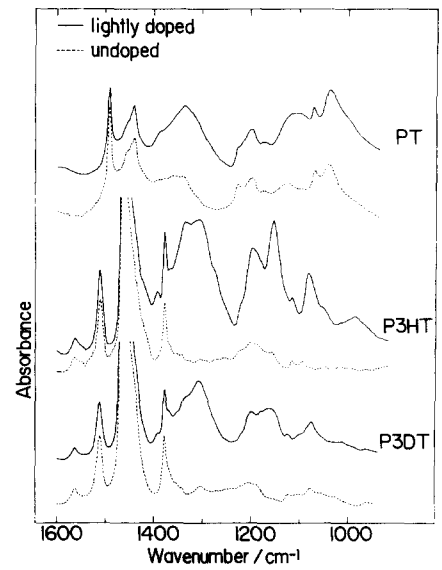

Figure 13 Comparison of infrared spectra before and after iodine doping in a series of P3AT samples

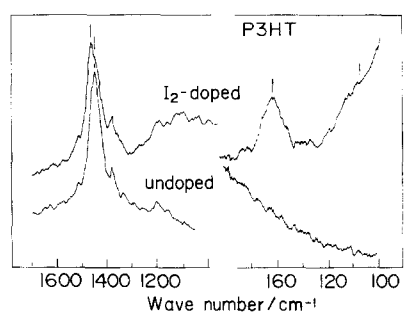

Figure 14 Raman spectral change before and after iodine doping of P3HT

polythiophene skeletal chain. An intense band is observed at 168 cm^{-1} only for the iodine-doped sample, which is assignable to the Raman bands of the I_5^- ion group[31,32]. The band at 108 cm^{-1}, characteristic of the I_3^- ion, is difficult to detect because of the disturbance of the band due to intense Rayleigh scattering. Therefore, at the present stage, it is not clear whether both the I_5^- and the I_3^- ions contribute to the complex formation.

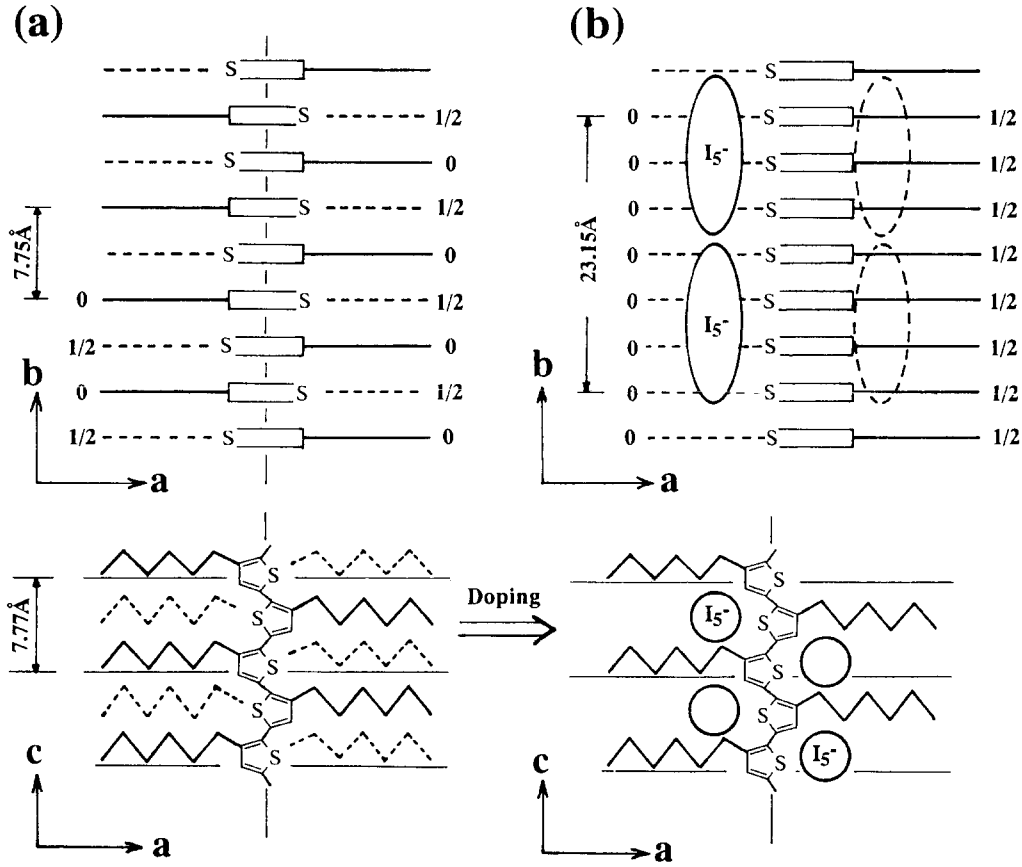

Figure 15 An illustrated crystal structural change induced by iodine doping

From all the data shown in *Figures 11–14*, we may speculate on the following structural change. Iodine groups penetrate into the crystalline lattice without any disturbance of the crystalline orientation and exist mainly in the form of I_5^- (and I_3^-) ion(s). The doping-induced chemical structural change of the skeletal chain is considered to occur in two stages, as seen in the infrared spectral change of *Figure 11*. These changes may correspond to the formation of polarons and bipolarons in the polythiophene skeletal chains. They might have large transition dipoles along the chain direction, as reasonably assumed from the parallel polarization character of the infrared bands (*Figure 12*). The electronic structure of these polarons and bipolarons is considered to differ between PT and P3HT, as seen in the large difference of the profile of the intense parallel bands, suggesting a strong influence of alkyl groups on the formation of the complex.

Crystal structural model of doped P3HT. As already mentioned, the size of the unit cell of the doped P3HT corresponds to that of six basic unit cells: two cells in the *a* direction and three cells along the *b* axis. The volume of the basic unit cell itself is approximately 1117 Å^3, which is ca. 120 Å^3 larger than the original unit cell volume, 1001 Å^3. The effective volume of one I_5^- ion is about 236 Å^3. Therefore the basic unit cell contains 0.5 I_5^- ions on average. In the parent unit cell, 3–4 I_5^- ions (4–5 I_3^- ions) are contained in total. That is, the molar ratio of the thiophene ring and the iodine ion is 6 : 1–8 : 1. This ratio is not unreasonable when compared with the value of 8 : 3 estimated from the weight change of the bulk sample measured before and after iodine doping, if such various factors as the trapping of iodine ions in the amorphous region are taken into consideration.

The X-ray diffraction and infrared/Raman spectral data require the following conditions for the construction of a model. (1) The cell constants change after doping but not very much: the *a*-axial length of the basic unit cell increases by ca. 2 Å, whereas the *b* and *c* axes are not greatly changed even after doping. These changes are dependent to some extent on the iodine concentration. (2) The skeletal polythiophene chain interacts with the iodine ions: that is, thiophene rings and iodine ions should be located at positions close to each other. (3) The alkyl side chains are basically kept unchanged, irrespective of the presence of iodine ions. (4) The space available for the location of iodine ions must be secured in the crystal lattice. By taking these important conditions into account, we proposed one possible model as shown in *Figure 15*, as reported in the previous paper[22]. In the crystal lattice of the original undoped sample (models 3 and 4), there is no space available for the iodine ions because the side chains are aggregated together in a close packing mode, as illustrated in *Figure 15a*. The spacing may be obtained reasonably, as shown in *Figure 15b*, by shifting the adjacent polythiophene chains along the chain axis by about one-half of the repeating period, and at the same time by effecting some degree of displacement along the *a* axis. As a result of such a translational displacement of the chains, tunnels are formed along the *b* axis, which can be used for creating one-dimensional chains of iodine ions. The thiophene ring and iodine molecule are located close to each other and therefore a relatively easy charge transfer might occur between these two groups, resulting in the generation of polarons

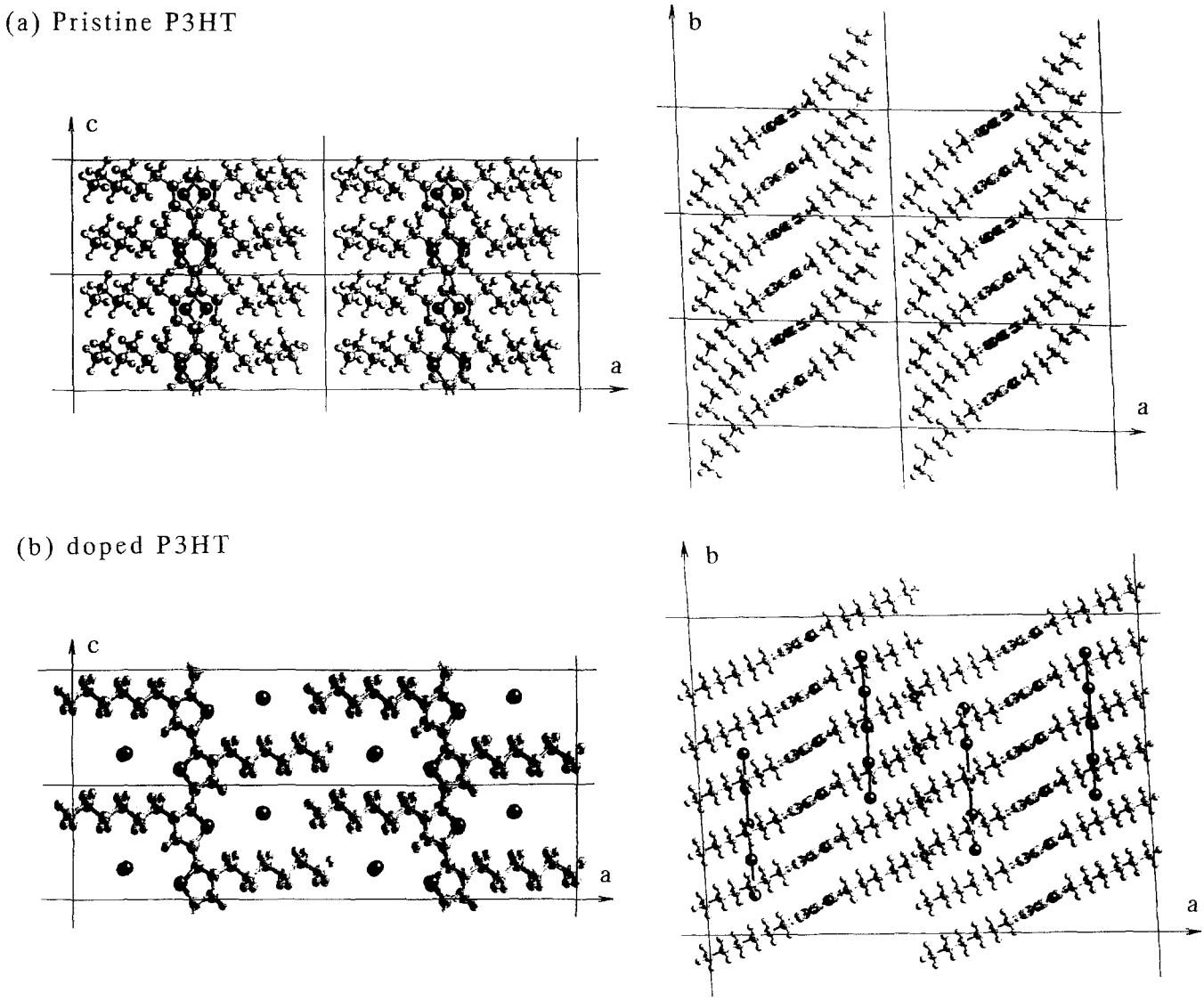

Figure 16 Energetically minimized crystal structures of (a) pristine and (b) iodine-doped P3HT. The pristine model is model 3, shown in *Figure 5*

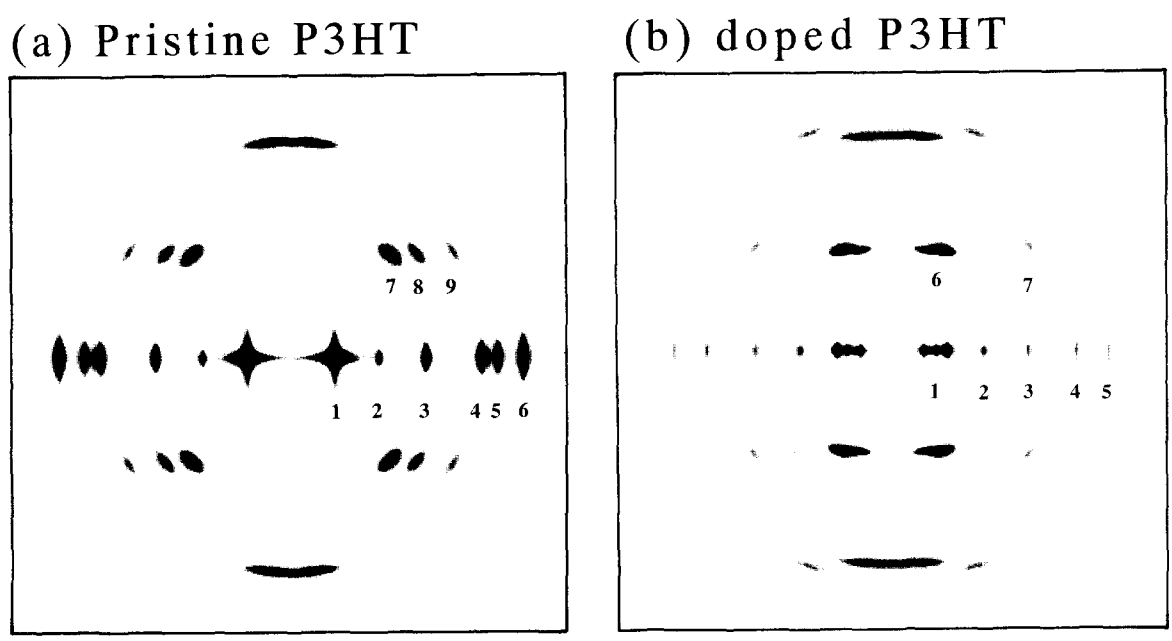

Figure 17 Comparison of X-ray fibre diagrams between pristine and iodine-doped P3HT samples. The models used are those shown in *Figure 16*. The numbering of the reflections corresponds to that shown in *Figure 10*

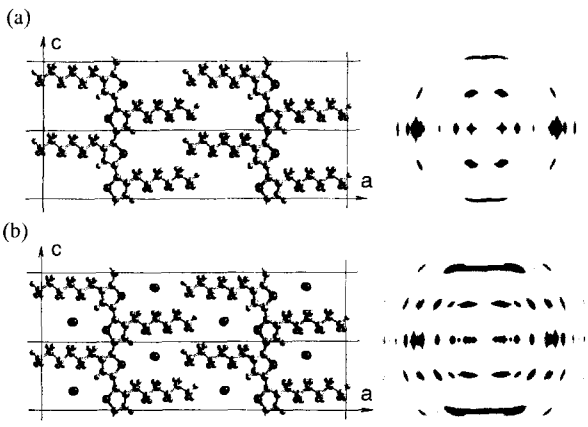

Figure 18 Comparison of X-ray fibre diagrams between P3HT models with and without iodine species in the crystal. The iodine-doped model is that shown in *Figure 16b* . In model (a), the iodine ions are removed from this doped model

and/or bipolarons. The idea of the *c*-axial translation of the chains is evidenced by the X-ray observation of the characteristic reflections (No. 6 in *Figure 10b*) for the doped sample, as explained below. After our paper proposing this structural change was published, we noticed that Winokur *et al.* reported essentially the same structural change for iodine-doped poly(3-octylthiophene) independently[7,23].

The above-mentioned idea of the structure has been checked by constructing a more realistic model by computer simulation. *Figure 16b* shows the model constructed for the doped P3HT in which the six basic cells of *Figure 16a*, taken from model 3 in *Figure 5*, are united together to form a superlattice cell. The iodine ions are packed along the *b* axis within the tunnels created by the cooperative translational shift of the chains along the *c* axis. The energetically minimized cell contains, as an example, $2I_5^-$ ions. The calculated cell parameters are $a = 35.08$ Å, $b = 25.10$ Å, $c = 7.83$ Å, $\alpha = 89.6°$, $\beta = 90.1°$ and $\gamma = 93.1°$, which may be said to correspond qualitatively to the observed values. Another model was constructed, also starting from model 4, the cell parameters of which are $a = 34.27$ Å, $b = 25.35$ Å, $c = 7.86$ Å, $\alpha = 89.8°$, $\beta = 89.8°$ and $\gamma = 90.3°$. In *Table 4* the observed lattice spacings and relative intensity are compared with those calculated for the model shown in *Figure 16b*. As to the reflectional intensities, the comparison can be made relatively reasonably as a whole, although some reflections give an appreciably large discrepancy between the observed and calculated tendencies (for example, Nos. 4, 7 and 8 in *Table 4*). The change in the X-ray fibre diagram is simulated, as shown in *Figure 17*, by using the structural models shown in *Figure 16*, where the numbering of the reflections corresponds to that shown in *Figure 10b*. The X-ray reflections of No. 6 in *Figure 10b*, which are characteristic of the doped sample and indexed as (*101*) and (*011*), can be simulated in the calculation.

Figure 18 shows the effect of the *c*-axial translation and that of the doped iodine ions on the X-ray diffraction pattern, where the model used is that shown in *Figure 16b*. Even if the iodine ions are removed from the doped model, the X-ray reflections (*101*) and (*011*) are still observed. In other words, the observation of these reflections, characteristic of the doped samples, indicates definitely the *c*-axial translation of the chains. By doping the iodine ions into this empty cell, many reflections are added to the fibre pattern (*Figure 18b*).

Winokur *et al.* proposed at first a structural model of iodine-doped poly(3-octylthiophene) in which mainly I_3^- ions are located within a cage formed by the four surrounding alkyl chains[7], but this model cannot be allowed stereochemically because no space is available for the iodine species. Afterwards they modified their model to that including the tunnels along the *b* axis which are created by shifting the chains along the chain axis[23]. This model is similar to that proposed in this section, but they doped mainly I_3^- ions so that the long axis of the ion becomes *parallel* to the alkyl side chain. In our case, on the other hand, the I_3^- and I_5^- ions are doped along the tunnel axis. Which is better for the location of iodine ions? In the model with the iodine ions oriented along the tunnels (*Figure 16*), the van der Waals radii of the iodine ions fit relatively well into the space of the tunnel. The length of the tunnel is infinite and so many iodine ions can be packed in a long array, just as is seen in the case of iodine-doped polyacetylene[33,34]; that is, the iodine ions can form very long polyiodine chains. When we constructed the model with the iodine ions oriented perpendicularly to the tunnels or along the alkyl chains, and carried out the energy calculation, the iodine ions were found to disturb the regularly arrayed alkyl chain layers. Besides, the poly(3-alkylthiophene) samples with short alkyl chains (for example, poly(3-butylthiophene), poly(3-propylthiophene) etc.) cannot hold the long iodine ions along the alkyl chain axis because the lengths of the I_3^- and I_5^- ions are ca. 10 Å and 17 Å respectively, which are too long compared with the alkyl chain lengths. As mentioned above, the iodide ions can exist in the various forms of I_2, I_3^-, I_5^- and I_7^-. The packing mode of iodine ions along the tunnel axis can accept these long molecules easily and without drastic structural change. It may be possible to check the orientation of the iodine molecules by measuring, for example, the polarized Raman spectra. In fact, the (*xy*) component of the polarized Raman spectra, in which the (*aa*), (*bb*) and (*ab*) components of the Raman polarizability tensor of the crystalline state are included, is more intensely observed than the (*zz*) component or the (*cc*) component, where the *z* axis is parallel to the *c* axis and the *x* and *y* axes are perpendicular to it. These polarized Raman data support, though only qualitatively, the above-mentioned idea on the orientation of the iodine ions.

At the present stage we cannot compare the observed and calculated X-ray diffraction patterns quantitatively but only semi-quantitatively, because the structural variables to be determined are too many compared with the observed number of reflections. But the essential feature of the crystal structure of the pristine and iodine-doped poly(3-alkythiophene)s can be said to be reproduced well by starting from models 3 and 4 with the *c*-axial shift of the chains forming long tunnels along the *b* axes.

REFERENCES

1. Winokur, M. J., Spiegel, D., Kim, Y., Hotta, S. and Heeger, A. J., *Synth. Met.*, 1989, **28**, C419.

2. Tashiro, K., Ono, K., Minagawa, Y., Kobayashi, M., Kawai, T. and Yoshino, K., *Synth. Met.*, 1991, **41–43**, 571.
3. Tashiro, K., Ono, K., Minagawa, Y., Kobayashi, M., Kawai, T. and Yoshino, K., *J. Polym. Sci., Part B: Polym. Phys.*, 1991, **29**, 1223.
4. Zerbi, G., Chierichetti, B. and Inganas, O., *J. Chem. Phys.*, 1991, **94**, 4646.
5. Tashiro, K., Minagawa, Y., Kobayashi, M., Morita, S., Kawai, T. and Toshino, K., *Synth. Met.*, 1993, **55–57**, 321.
6. Tashiro, K., Minagawa, Y., Kobayashi, M., Morita, S., Kawai, T. and Yoshino, K., *Rep. Progr. Polym. Phys. Jpn*, 1992, **35**, 464.
7. Winokur, M. J., Wamsley, P., Moulton, J., Smith, P. and Heegar, A. J., *Macromolecules*, 1991, **24**, 3812.
8. Mardalen, J., Samuelsen, E. J., Gantun, O. R. and Garlsen, P. H., *Synth. Met.*, 1992, **48**, 363.
9. Fell, H. J., Samuelsen, E. J., Bakken, E. and Carlsen, P. H. J., *Synth. Met.*, 1995, **72**, 193.
10. Hsu, W.-P., Levon, K., Ho, K.-S., Kwei, T. K. and Myerson, A. S., *Macromolecules*, 1993, **26**, 1318.
11. Mardalen, J., Samuelsen, E. J., Gautun, O. R. and Carsen, P. H., *Solid State Commun.*, 1991, **77**, 337.
12. Mardalen, J., Samuelsen, E. J., Gautun, O. R. and Carsen, P. H., *Solid State Commun.*, 1991, **80**, 687.
13. Ihn, K. J., Moulton, J. and Smith, P., *J. Polym. Sci.: Part B: Polym. Phys.*, 1993, **31**, 735.
14. Kawai, T., Nakazono, M. and Yoshino, K., *J. Mater. Chem.*, 1992, **2**, 903.
15. Bolohnesi, A., Catellani, M., Destri, S. and Porzio, W., *Makromol. Chem., Rapid Commun.*, 1991, **12**, 9.
16. Gustafsson, G., Inganas, O., Osterholm, H. and Laakso, J., *Polymer*, 1991, **32**, 1574.
17. Kawai, T., Nakazono, M., Sugimoto, R. and Yoshino, K., *J. Phys. Soc. Jpn*, 1992, **6**, 3400.
18. McCullough, R., Tristram-Nagle, S., Williams, S., Lowe, R. and Jayaraman, M., *J. Mater. Chem.*, 1992, **2**, 903.
19. Prosa, T. J., Winokur, M. J., Moulton, J., Smith, P. and Heeger, A. J., *Macromolecules*, 1992, **25**, 4364.
20. Luzny, W., *Acta Cryst.*, 1995, **B51**, 255.
21. Onoda, M., Manda, Y., Morita, S. and Yoshino, K., *J. Phys. Soc. Jpn*, 1989, **58**, 1895.
22. Tashiro, K., Minagawa, Y., Kobayashi, M., Morita, S., Kawai, T. and Yoshino, K., *Jpn J. Appl. Phys.*, 1994, **33**, L1023.
23. Prosa, T. J., Winokur, M. J., Moulton, J., Smith, P. and Heeger, A., *J. Phys. Rev. B.* 1995, **51**, 159.
24. Tashiro, K., Asanaga, H., Ishino, K. and Kobayashi, M., *Prepr. Polym. Soc. Jpn*, 1996, **45**, 793.
25. Tashiro, K., Ishino, K., Kobayashi, M. and Asanaga, H., *Prepr. Polym. Soc. Jpn*, 1996, **45**, 3302.
26. Tashiro, K., Tazaki, R., Ishino, K., Kobayashi, M. and Asanaga, H., *Polym. Prepr. Jpn*, 1995, **44**, 3087.
27. Tashiro, K. and Kobayashi, M., *Proceedings of the Osaka University Macromolecular Symposium*, Springer Verlag, 1994, p. 17.
28. Tashiro, K., Kobayashi, M., Morita, S., Kawai, T. and Yoshino, K., *Rep. Progr. Polym. Phys. Jpn*, 1994, **37**, 225.
29. Mayo, S. L., Olafson, B. D. and Goddard, W. A. III, *J. Phys. Chem.*, 1990, **94**, 8897.
30. Rappe, A. K. and Goddard, W. A. III, *J. Phys. Chem.*, 1991, **95**, 3358.
31. Mizuno, M., Tanaka, J. and Harada, I., *J. Phys. Chem.*, 1981, **85**, 1789.
32. Inagaki, F., Harada, I., Shimanouchi, T. and Tasumi, M., *Bull. Chem. Soc. Jpn.*, 1972, **45**, 3384.
33. Murthy, N. S., Miller, G. G. and Baughman, R. H., *J. Chem. Phys.*, 1988, **89**, 2523.
34. Albony, P. A., Pouget, J. P., Halim, J., Enkelman, V. and Wegner, G., *Makromol. Chem.*, 1992, **193**, 853.